ACS APPLIED MATERIALS & INTERFACES

Research Article

www.acsami.org

Role of Thin n-Type Metal-Oxide Interlayers in Inverted Organic Solar Cells

Abay Gadisa,*[,†] Yingchi Liu,[‡] Edward T. Samulski,[†] and Rene Lopez[‡]

[†]Department of Chemistry, University of North Carolina at Chapel Hill, Caudill and Kenan Laboratories CB 3290 Chapel Hill, North Carolina 27599, United States

[‡]Department of Physics and Astronomy, University of North Carolina at Chapel Hill, Phillips Hall CB 3255, Chapel Hill, North Carolina 27599, United States

Supporting Information

ABSTRACT: We have investigated the photovoltaic properties of inverted solar cells comprising a bulk heterojunction film of poly(3-hexylthiophene) and phenyl-C_{61}-butyric acid methyl ester, sandwiched between an indium−tin-oxide/Al-doped zinc oxide (ZnO-Al) front, and tungsten oxide/aluminum back electrodes. The inverted solar cells convert photons to electrons at an external quantum efficiency (EQE) exceeding 70%. This is a 10−15% increase over EQEs of conventional solar cells. The increase in EQE is not fully explained by the difference in the optical transparency of electrodes, interference effects due to an optical spacer effect of the metal-oxide electrode buffer layers, or variation in charge generation profile. We propose that a large additional splitting of excited states at the ZnO−Al/polymer interface leads to the considerably large photocurrent yield in inverted cells. Our finding provides new insights into the benefits of n-type metal-oxide interlayers in bulk heterojunction solar cells, namely the splitting of excited states and conduction of free electrons simultaneously.

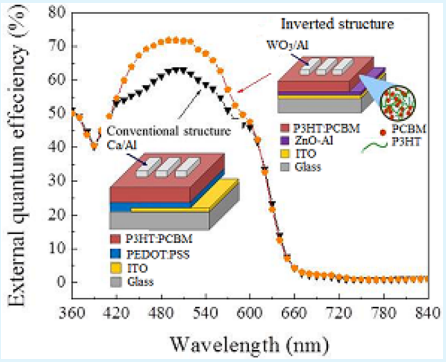

KEYWORDS: *Al-doped ZnO, bulk heterojunction, photocurrent, metal oxide, inverted solar cell*

INTRODUCTION

Polymeric semiconductors exhibit great potential for energy conversion in photovoltaic devices. They offer unique properties that enable easy processing from liquid solutions, thereby allowing for low-cost cell manufacturing over large surface areas via roll-to-roll manufacturing. Polymer solar cells (PSC) are composed of a bulk heterojunction (BHJ) photoactive film formed by mixing semiconducting polymers with electron acceptor molecules such as fullerenes. A photocurrent is primarily generated through dissociation of excited states at the polymer/fullerene interfaces, followed by the transfer of electrons to the fullerene molecule.[1] Charge generation and collection processes are highly dependent on the active layer morphology. BHJ films must form a phase separated morphology, characterized by length scales on the order of exciton diffusion length (~5−10 nm) while maintaining bicontinuous percolation paths for the free charge carriers.[1−4] BHJ solar cells with internal efficiencies of nearly 100% have been realized upon careful selection of material combinations and improved BHJ morphology.[5] Power conversion efficiency can also be improved through reduction of parasitic losses originating from reflection[6] or energy dissipation in nonexciton generating layers.[7]

Electrodes and buffer layers play pivotal roles in realizing efficient, stable and robust PSCs. Conventional PSCs are built on top of an indium−tin-oxide (ITO) anode, which is often covered by a buffer layer, typically poly(3,4-ethylenedioxythiophene):poly(styrene-sulfonate) (PEDOT:PSS).[3−6] PEDOT:PSS is a moderately conducting polymer with high optical transparency.[8] However, it is inherently acidic and may etch the ITO electrode leading to indium diffusion into the polymer active layer.[9] In addition, its hygroscopic nature may initiate device degradation. Some reports have shown that PEDOT:PSS is also an inefficient electron-blocking layer, reducing the efficiency of electronic devices through electron leakage to the anode electrode.[10] For these reasons, alternative high work function electrodes have been explored and demonstrated by essentially replacing PEDOT:PSS with metal-oxides such as molybdenum oxide (MoO_3),[11] tungsten oxide (WO_3),[12] vanadium oxide (V_2O_5),[13] and nickel oxide (NiO).[14] Similarly, highly reactive low work function metal electrodes, which are commonly used in PSCs, have been effectively replaced by electron transporting metal-oxides such as TiOx[5,15] and ZnO.[16]

The power conversion efficiency of polymer-based solar cells has been increasing dramatically over the past few years, currently exceeding 8%.[17] This is primarily due to increased knowledge of the morphological changes imparted by film processing, utilization of more robust materials, and use of better electrodes. These advances, together with increased

Received: March 28, 2012
Accepted: July 16, 2012
Published: July 26, 2012

lifetimes,[18] bring PSCs closer to commercialization. Of particular interest are recent reports that have shown the achievement of longer lifetimes in inverted solar cells.[19,20] Optimized inverted solar cells deliver respectable power conversion efficiencies. For example, inverted solar cells with an active layer of poly(3-hexylthiophene) and a fullerene derivative molecule indene-C_{60} bis-adduct has been shown to exhibit an efficiency of 6.2%,[21] while a blend of a low bandgap polymer poly[N-9″-hepta-decanyl-2,7-carbazole-alt-5,5-(4′,7′-di-2-thienyl-2′,1′,3′-benzothiadiazole)] and a fullerene derivative [6,6]-phenyl C_{70}-butyric acid methyl ester delivered an efficiency of 6.3%.[19] A certified 7.4% power conversion efficiency was recently published by C. E. Small et al.,[22] which affirms the competitiveness of inverted solar cells with conventional structures. Most inverted solar cells are also known to yield more photocurrent relative to conventional solar cells.[23−25] There have been several explanations in recent reports for the observed photocurrent increment in inverted cells. Typically, the increased photocurrent was attributed to improved optical transmittance,[23,26] and improved charge collection efficiency.[24] However, it has been noted that unlike in the conventional PSCs,[5] the thin metal-oxide layers of inverted solar cells exhibit negligible positive optical spacer effects.[26]

In this study, we discuss the photovoltaic properties of the bulk heterojunction layer of poly(3-hexylthiophene) (P3HT) and phenyl-$C6_1$-butyric acid methyl ester (PCBM) in inverted structures employing glass/ITO/Al-doped zinc-oxide (ZnO-Al) cathode, and a tungsten-oxide (WO_3)/aluminum anode. Inverted solar cells with an ∼80 nm blend layer convert incident photons to electrons at external quantum efficiency (EQE) exceeding 70%. The EQE of similarly made and optimized conventional cells, with an ITO/PEDOT:PSS anode and a Ca/Al cathode, barely exceeds 60%. The conductivity and optical transparency (and reflection) of electrodes were shown to have some minor effects on photocurrent yield.[23,26] Here, we present strong evidence demonstrating that the extra current generated in inverted solar cells originates primarily from the photocarriers generated by the dissociation of excited states at the metal-oxide/P3HT interfaces. We discuss our findings derived from photovoltaic, photoluminescence, and optical characterizations of photovoltaic devices utilizing a P3HT:PCBM photoactive layer and glass/ITO/ZnO-Al, or glass/ITO/PEDOT:PSS bottom electrode.

EXPERIMENTAL SECTION

Device Preparation. Inverted solar cells were built on glass/ITO (140 nm) substrates covered with a ZnO-Al layer, which was deposited using a pulsed laser deposition (PLD) technique. The PLD technique offers capabilities for making uniform and reproducible films. The deposition of ZnO-Al was performed at a temperature of 200 °C under 10 mTorr O_2 pressure, using a ZnO:Al2O_3 (98/2 wt %) target. The glass/ITO substrates were thoroughly cleaned using acetone and isopropanol prior deposition of the ZnO-Al layers. The thickness of the ZnO-Al layer was typically ∼50 nm. Conventional solar cells were also built on glass/ITO substrates, which were covered by a ∼30 nm thick PEDOT:PSS (CLEVIOS P VP AI 4083) layer. A solution of P3HT/PCBM (1:0.8, wt.%) was spin-casted on the substrates from a 18 mg/mL 1,2-dichlorbenzene solution. Partially wet blend BHJ films were allowed to dry in closed Petri-dishes for about 10 to 15 min and subsequently thermally annealed at a temperature of 140 °C for 10 min. The resulting blend film was ∼80 nm thick. The P3HT and PCBM were purchased from Rieke metals and Nano C, respectively, and used as received. Finaly, Tungsten oxide (WO_3, 3 nm) and aluminum (100 nm) layers were subsequently thermally evaporated on top of the active layers under a shadow mask in a base pressure of 1×10^{-6} mbar. For conventional cells, a calcium (10 nm)/Al (100 nm) electrode was thermally deposited on top of the blend layer. Inverted or conventional only P3HT-based photocells were also fabricated following the same procedures. The P3HT was casted from a chlorobenzene solution and gives a thickness of ∼40 nm. For photoluminescence measurements, pure P3HT film (∼ 25 nm) was casted on a glass substreate which was partially covered with a layer of ZnO-Al. All P3HT films were annealed at a temperature of 140 °C for 10 min.

Measurements. Current−voltage characteristics of the solar cells were measured using a Keithley 2400 source meter. The photovoltaic characteristics of the solar cells were recorded under a simulated A.M. 1.5G (1000 W/m^2) solar illumination from a Newport solar simulator. To measure an external quantum effeciency, a photocurrent generated by an incident chopped monochromatic light was recorded using a lockin amplifier. The procesing and characterization of the solar cells were all done in a nitrogen filled glovebox (H_2O < 0.1 PPM; O_2 < 0.1 PPM). Optical transmission measurements were done using a normal incidence reflection/transmission upright microscope with a conventional 4x microscope objective. Reflected light was collected by an optical fiber and analyzed with a monochromator equipped with a cooled CCD array. The light source and optical setup were normalized to a UV-enhanced aluminum mirror. Photoluminescence (PL) measurements of P3HT-only samples were done in a similar fashion but replacing the light source with a 532 nm CW laser light (∼2 mW) and adding a 532 line filter in the incident light path and a complementary 532 long-pass filter. Importanty, the sample was mounted in a microscope-compatible vacuum chamber (base pressure 1×10^{-5} mbar) to prevent PL degradation originating from quenching of excited states by oxygen.[27] PL spectra recorded in air degrades with time, which would have made comparative studies impossible.

RESULTS AND DISCUSSION

Our investigation is focused on fabricating and characterizing inverted and conventional solar cells having an 80 nm thick P3HT:PCBM (1:0.8, wt.) photoactive film. This thickness was chosen for two reasons. First, the first P3HT optical interference maxima falls within this range.[28] Second, according to our previous report, the electron and hole transport lengths (340, and 90 nm, respectively) for the P3HT:PCBM blend film exceed the 80 nm film thickness.[29] This implies that the number of charges collected at electrodes should remain comparable for the inverted and conventional solar cells assuming the BHJ film morphology remains similar in both devices. For simplicity, the studied devices are identified as follows:

- Device **1**: glass/ITO/PEDOT:PSS/P3HT:PCBM/Ca/Al (conventional structure)
- Device **2**: glass/ITO/ZnO-Al/PEDOT:PSS/P3HT:PCBM/Ca/Al (conventional structure)
- Device **3**: glass/ITO/ZnO-Al/P3HT:PCBM/WO_3/Al (inverted structure)

The photovoltaic characteristics of all devices are displayed in Figure 1. Both the inverted and conventional cells exhibit good performance (η_e ∼3.6 vs 4.6%), typical of P3HT:PCBM based solar cells. A 10−15% increase in photocurrent yield was measured in the inverted cells (Device **3**) compared to the reference conventional cell (Device **1**). This result is one of the best ever recorded for PSCs having a ZnO-Al front electrode.[25]

The open-circuit voltage (V_{oc}) and fill factor (FF) of the inverted solar cells are, however, reduced compared to that of the conventional cells. The decrease in FF and V_{oc} are currently under investigation. Preliminary results indicate that intrinsic traps within the ZnO-Al layer as well as backflow of charges

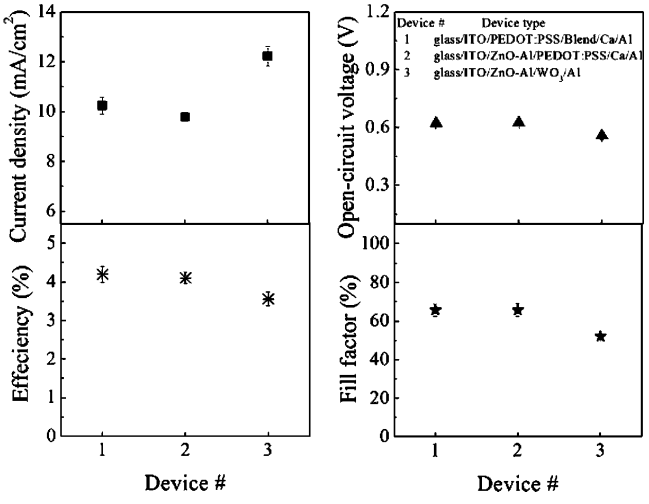

Figure 1. Photovoltaic parameters of ITO/PEDOT:PSS/P3HT:PCBM/Ca/Al (Device 1), ITO/ZnO-Al/PEDOT:PSS/P3HT:PCBM/Ca/Al (Device 2) and ITO/ZnO-Al/P3HT:PCBM/WO_3/Al (Device 3).

may play crucial roles in the reduction of FF and V_{oc} in the inverted devices. In order to corroborate this we have converted one of the inverted solar cells to a conventional cell architecture by casting a 30 nm PEDOT:PSS layer on top of the glass/ITO/ZnO-Al substrate (Device **2**). As shown in Figure 1 the performance of this particular device is nearly equal to that of the conventional reference cell (Device **1**), and both the FF and V_{oc} are now considerably increased. It is, noted, however that J_{sc} is decreased when PEDOT:PSS was in the inverted cell as in Device-**2**. Open circuit-voltages of BHJ devices are mainly determined by the energy of the polymer/fullerene interfacial charge transfer states in devices with perfectly conducting and ohmic electrodes.[30−33] As our main concern is focused on the origin of photocurrent increment, the differences in V_{oc} and FF do not affect our analysis and conclusions.

The photocurrent enhancement is evident in the external quantum efficiency of the devices as shown in Figure 2. The EQE spectra show that the photocurrent increase is realized throughout all regions where P3HT absorbs. The EQE of the inverted solar cells exceeds 70%, which is typical of other inverted solar cells.[25,26] The conventional cell may suffer from optical loses in the PEDOT:PSS layer since it is not perfectly transparent in the visible sun energy spectrum. This seems to support the typical explanation of better optics as the reason for larger short-circuit current (J_{sc}) in inverted solar cells. According to previous reports, the increased photocurrent recorded in inverted solar cells was attributed to improved optical transmittance,[23,26] and improved charge collection efficiency.[24] To explore the origin of current increase in inverted cells in more detail, we have characterized the optical transmission and reflection spectra of the front electrodes as well as that of the complete solar cell devices (See Figure 3).

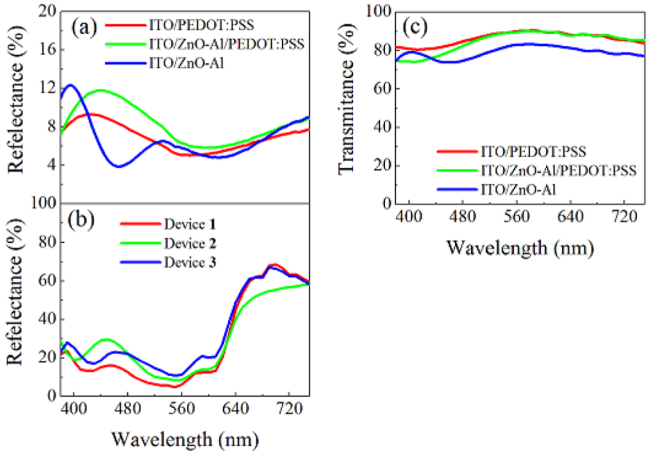

Figure 3. Reflection characteristics of (a) the various front electrodes and (b) full solar cell devices. The transmission spectra of the front electrodes are displayed in (c). All the measurements were carried out at normal incidence.

The front electrodes of Device **1** and Device **2** have very similar transmission in the high wavelength region (>∼550 nm). Below 550 nm, the contact of Device **2** is less transparent and more reflective. On the other hand, the contact of Device **3** is less transparent in the wavelength region exceeding ∼450 nm compared to the contacts of both Device **1** and **2**. Device **2** has a somewhat higher reflection response, and this has probably

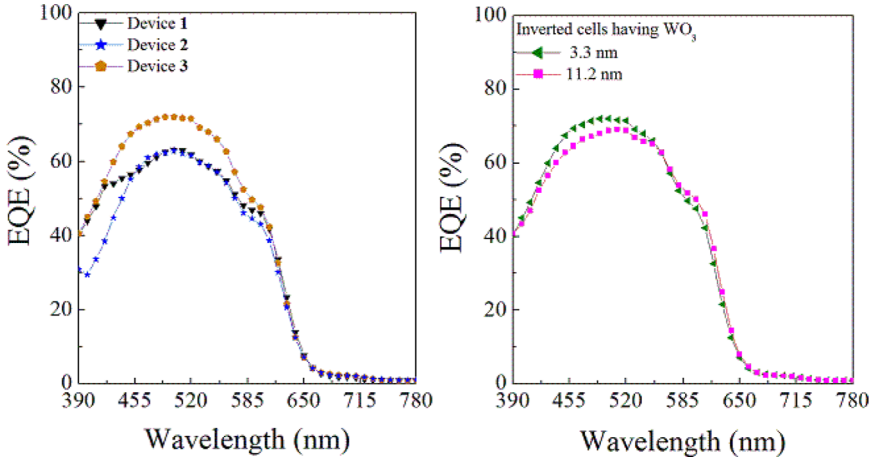

Figure 2. External quantum efficiency (EQE) spectra of ITO/PEDOT:PSS/P3HT:PCBM/Ca/Al (Device 1), ITO/ZnO-Al/PEDOT:PSS/P3HT:PCBM/Ca/Al (Device 2), and ITO/ZnO-Al/P3HT:PCBM/WO_3/Al (Device 3) (left figure). The inverted devices show higher EQE as compared to the conventional devices. The figure in the right represents EQEs of two inverted solar cells having WO_3 layers of different thicknesses.

contributed to its reduced photocurrent as compared to the inverted cell. However, the overall photovoltaic performance of Device **2** is nearly equivalent to that of the reference cell except for the slightly smaller photocurrent, which may be assumed to be in accord with the measured differences in their optical full device reflection losses (Figure 3b). Thus, the trend of the measured optical transparency and reflection is not in a linear correlation with the observed increase in photocurrent in inverted devices. In the complete devices, the incident light intensity distribution within the organic film is strongly dictated by reflection and interferences. The latter is directly correlated with the total number of absorbed photons within the active layer. To consider these optical effects, we have calculated the total number of absorbed photons in each complete cell using the transfer matrix method. The total number of absorbed photons in the cells is nearly equivalent as shown in Figure 4a.

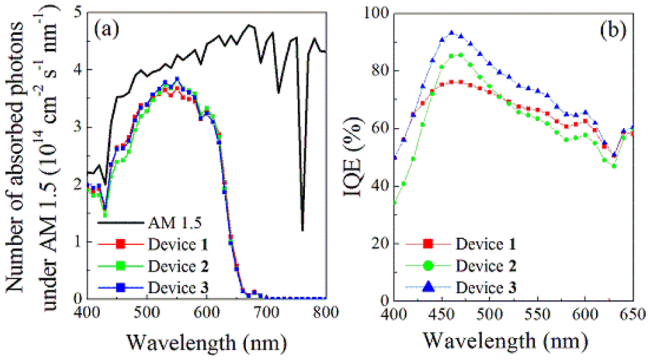

Figure 4. (a) Total number of photons absorbed in each device, and (b) the corresponding internal quantum efficiency.

However, the internal quantum efficiency (IQE) shows a clear difference as depicted in Figure 4b. IQE is described by exciton diffusion, charge transfer, and charge collection effeciencies.[34] Device **3** has a significantly larger IQE in comparison to that of Device **1** and **2**. Comparing the IQEs of Devices **1** and **2**, one recognizes no clear overall difference but they have differing IQEs at various regions of the solar spectra.

Interfacial buffer layers in the back contact, such as WO_3, may act as optical spacers as well and manipulate the optical interference within the active layer.[5] Although this was found to be negligible for inverted solar cells with thin back oxide layers,[26] we have used a 3 - 4 nm thick WO_3 layer in order to reduce the optical spacer effect, if, in fact, there is one. We have, however, observed a small photocurrent reduction (~1−2%) on changing the WO_3 thickness from 3 to 11 nm. (See Figure 2, right) Moreover, as discussed previously, the fact that the carrier transport lengths exceeded the active layer thickness[29] implies negligible differences in the number of free carriers reaching the electrodes. We have previously shown that this scenario will change for thick films as more holes start to be generated near the back electrode[29] and in this case the conventional reference cell starts to produce more current than the inverted cell. Overall then, we see minor differences from an optical perspective, and therefore incapable of explaining the enhanced current in inverted devices.

In order to explain the extra-current, we have looked at the problem from a different perspective. ZnO is a known electron accepting and transporting material.[21,25,33] We have made a systematic study of the charge transfer characteristics of glass/ZnO-Al/P3HT samples using emission spectroscopy. The latter involved recording of the photoluminescence (PL) properties of P3HT films cast on a glass substrate with one-half-coated with a ZnO-Al layer. Excitation and collection of PL emitted light was performed on the P3HT film side in order to avoid effects of light scattering through the substrates. The laser excitation wavelength is near the maximum absorption peak of P3HT (550 nm), whereas it is not absorbed at all by the ZnO layer. The PL data recorded by probing at various locations of the sample are shown in Figure 5. A substantial reduction in PL intensity was recorded in the presence of the ZnO-Al film. Although the P3HT:PCBM BHJ films exhibit complete quenching, we believe that P3HT chains lying near the ZnO-Al interface may preferentially transfer electrons to the ZnO-Al layer thereby producing a photocurrent. The availability of pure P3HT at the ZnO-Al interface is plausible since vertical phase separation is known to occur in films of polymer/PCBM blend.[35] Vertical phase separation in BHJ films of inverted cells has recently been under discussions. Y. Vaynzof et al.[36] have shown formation of 1−2 nm PCBM-rich layer at a ZnO/P3HT:PCBM interface, whereas the same amount of P3HT-rich layer was found at the air interface. This conclusion was reached based on XPS depth profile and UPS studies. On the

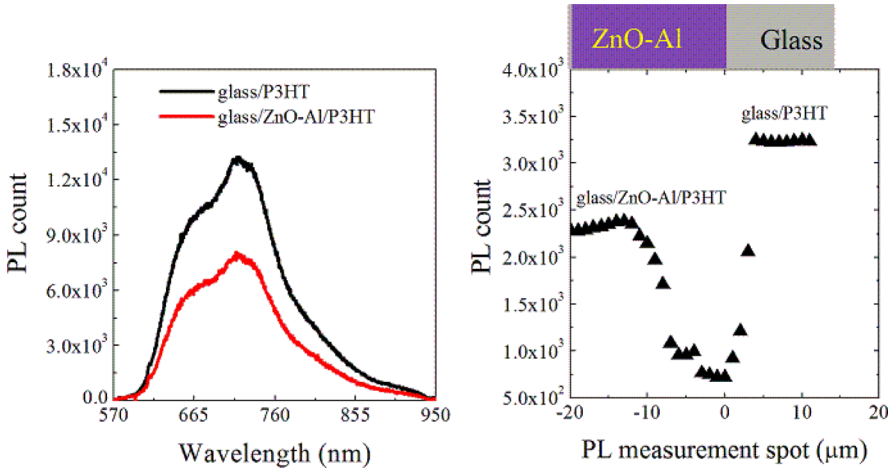

Figure 5. Photoluminescence spectra of P3HT film casted on a glass substrate half-covered with a 50 nm ZnO−Al layer. The dip in the right PL curve is due to a scratch on the P3HT film to mark the ZnO boundary.

contrary, using an XPS depth profile analysis, H. Cheun et al.[37] have recently shown a preferential enrichment of a P3HT-rich phase adjacent to the bottom ZnO substrate. The latter report suggested that the relatively hydrophobic nature of the ZnO layer (contact angle about 64°) may agitate P3HT to segregate toward the ZnO layer, which is also consistent with other reports (ref 34). We have measured the contact angle of ITO/PEDOT:PSS and ITO/ZnO-Al substrates and found a value of 9 and 62°, respectively. The relatively hydrophobic ZnO-Al substrate may allow accumulation of more P3HT chains near the ZnO-Al/Blend interface compared to the highly hydrophilic PEDOT layer. The observed quenching of excited states at the ZnO-Al/P3HT interface should yield photocurrent in solar cells. With the aim of exploring the extent of this interface generated current, two types of solar cells comprsing ~40 nm of P3HT layer were made, viz. ITO/PEDOT:PSS/P3HT/Ca/Al and ITO/ZnO-Al/P3HT/WO_3/Al. The first cell is not expected to produce substantial current since no exciton quenching layer is included in the cell. This indeed is the case as observed from the experimental result displayed in Figure 6.

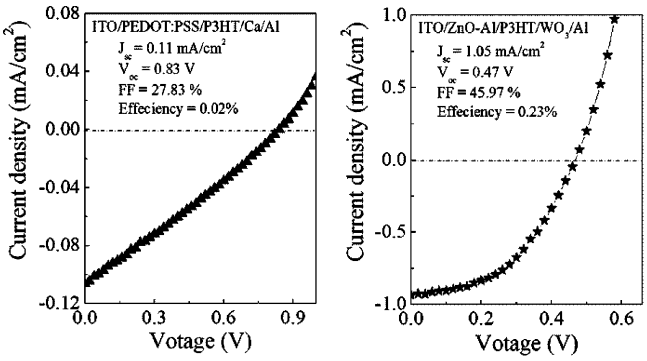

Figure 6. Photovoltaic characteristics of solar cells comperising only P3HT as a photoactive layer-ITO/PEDOT:PSS/P3HT/Ca/Al (left) and ITO/ZnO-Al/P3HT/WO_3/Al (right).

The inverted solar cell has resulted into a 10-fold increase in photocurrent yield and a decent fill factor. The photocurrent generated at the ZnO-Al/P3HT interface, however, is subject to losses mainly due to back recombination as reported previously.[38−41] This losses can be remedided through interfacial modifications.[40,41] The aforementioned loss has been observed for our ZnO-Al/P3HT device. Clear changes in photocurrent were observed after an ultrathin layer of a ruthinium dye N719 was adsorbed onto the ZnO-Al layer (see Figure 2S in the Supporting Information). N719 forms a dipole at the P3HT/ZnO-Al interface, which shifts the interface energy offset resulting in reduced charge backflow.[40,41] According to a recent report, a simple interfacial engineering of a BHJ inverted solar cell has resulted into an effeciency surpassing 8%, whereas a 6.1% effeciency was achieved in nonmodified devices.[42] In general, despite the observed loss, the photocurrent generated at the ZnO-Al/polymer bilayer almost approaches the photocurrent change observed earlier between the inverted and conventional bulk heterojunction devices. These results imply that thin films of n-type metal-oxides, integrated into BHJ organic solar cells, have potential for quenching excited states created at the metal-oxide/polymer interface. Moreover, the electrons that are directly transferred to the metal-oxide are the most effectively collected since losses are minimum compared to the ones created in the bulk of the BHJ material through exciton quenching at the PCBM/polymer interfaces. This apparent multifunctionality of the metal-oxide layers is a very important characteristic which has not been previously considered in BHJ based solar cells. This attractive feature of the inverted solar cells could be benefecial for fabrication of cost-effective thin layer organic solar cells if the detrimental aspects of the inverted architecture can be ameliorated.

CONCLUSIONS

Inverted solar cells with glass/ITO/ZnO-Al transparent front electrodes convert incident photons to electrons at an efficiency exceeding 70%. We have shown that, compared to conventional cells with ITO/PEDOT:PSS anode, the inverted cells yield more photocurrent primarily due to a high probability of additional carrier generation at the ZnO-Al/P3HT interface. This investigation gives new insights into the role of metal-oxide layers in BHJ organic solar cells.

ASSOCIATED CONTENT

Supporting Information

Calculated total and measured reflectance of conventional and inverted solar cells, and the external quantum efficiency of ZnO-Al/P3HT solar cells. This material is available free of charge via the Internet at http://pubs.acs.org.

AUTHOR INFORMATION

Corresponding Author

*E-mail: abay@unc.edu or abaymy@yahoo.com.

Notes

The authors declare no competing financial interest.

ACKNOWLEDGMENTS

Support for this work from NSF (Solar: DMR-0934433) is gratefully acknowledged.

REFERENCES

(1) Yu, G.; Gao, J.; Hummelen, J. C.; Wudl, F.; Heeger, A. J. *Science* **1995**, *270*, 1789−1791.
(2) Halls, J. J. M.; Walsh, C. A.; Greenham, N. C.; Marseglia, E. A.; Friend, R. H.; Holmes, A. B. *Nature* **1995**, *376*, 498−500.
(3) Gadisa, A.; Mammo, W.; Andersson, L. M.; Admassie, S.; Zhang, F.; Andersson, M. R.; Inganäs, O. *Adv. Funct. Mater.* **2007**, *17*, 3836−3842.
(4) Chen, H.-Y.; Hou1, J.; Zhang, S.; Liang, Y.; Yang, G.; Yang, Y.; Yu, L.; Wu1, Y.; Li, G. *Nat. Photon.* **2009**, *3*, 649−653.
(5) Park, S. H.; Roy, A.; Beaupré, S.; Cho, S.; Coates, N.; Moon, J. S.; Moses, D.; Leclerc, M.; Lee, K.; Heeger, A. J. *Nat. Photon.* **2009**, *3*, 297−302.
(6) Hadipour, A.; Cheyns, D.; Heremans, P.; Rand, B. P. *Adv. Energy Mater.* **2011**, *1*, 930−935.
(7) Pettersson, L. A. A.; Roman, L. S.; Inganas, O. *J. Appl. Phys.* **1999**, *86*, 487−496.
(8) Kim, Y. H.; Sachse, C.; Machala, M. L.; May, C.; Meskamp, L. M.; Leo, K. *Adv. Funct. Mater.* **2011**, *21*, 1076−1081.
(9) Chen, L.-M.; Hong, Z.; Li, G.; Yang, Y. *Adv. Mater.* **2009**, *21*, 1434−1449.
(10) (a) Yan, H.; Lee, P.; Armstrong, N. R.; Graham, A.; Evmenenko, G. A.; Dutta, P.; Marks, T. J. *J. Am. Chem. Soc.* **2005**, *127*, 3172−3183. (b) Kim, Y. H.; Lee, S.-H.; Noh, J.; Han, S.-H. *Thin Solid Films* **2006**, *510*, 305−310.
(11) Tokito, S.; Noda, K.; Taga, Y. *J. Phys. D: Appl. Phys.* **1996**, *29*, 2750−2753.
(12) Meyer, J.; Hamwi, S.; Bülow, T.; Johannes, H.-H.; Riedl, T.; Kowalsky, W. *Appl. Phys. Lett.* **2007**, *91*, 113506(1)−113506(3).

(13) Shrotriya, V.; Li, G.; Yao, Y.; Chu, C. W.; Yang, Y. *Appl. Phys. Lett.* **2006**, *88*, 073508(1)−073508(3).
(14) Irwin, M. D.; Buchholz, D. B.; Hains, A. W.; Chang, R. P. H.; Marks, T. J. *Pro. Natl. Acad. Sci.* **2008**, *105*, 2783−2787.
(15) Steim, R.; Choulis, S. A.; Schilinsky, P.; Brabec, C. J. *Appl. Phys. Lett.* **2008**, *92*, 093303(1)−093303(3).
(16) Gilot, J.; Wienk, M. M.; Janssen, R. A. J. *Appl. Phys. Lett.* **2007**, *90*, 143512(1)−143512(3).
(17) Green, M. A.; Emery, K.; Hishikawa, Y.; Warta, W.; Dunlop, E. D. *Prog. Photovolt: Res. Appl.* **2011**, *19*, 565−572.
(18) Peters, C. H.; S.-Quintana, I. T.; Kastrop, J. P.; Beaupré, S.; Leclerc, M.; McGehee, M. D. *Adv. Energy Mater.* **2011**, *1*, 491−494.
(19) Sun, Y.; Seo, J. H.; Takacs, C. J.; Seifter, J.; Heeger, A. J. *Adv. Mater.* **2011**, *23*, 1679−1683.
(20) (a) Dey, S.; Vivo, P.; Efimov, A.; Lemmetyinen, H. *J. Mater. Chem.* **2011**, *21*, 15587−15592. (b) Huang, J.-S.; Chou, C.-Y.; Lin, C.-F. *IEEE Electron Device Lett.* **2010**, *31*, 332−334.
(21) Cheng, Y.-J.; Hsieh, C.-H.; He, Y.; Hsu, C.-S.; Li, Y. *J. Am. Chem. Soc.* **2010**, *132*, 17381−17383.
(22) Small, C. E.; Chen, S.; Subbiah, J; Amb, C. M.; Tsang, S.-W.; Lai, T.-H.; Reynolds, J. R.; So, F. *Nat. Photon.* **2012**, *6*, 115−120.
(23) Sio, A.; De; Chakanga, K.; Sergee, O.; Maydell, K.; von; Parisi, J.; Hauff, E. von *Sol. Energy Mater. Sol. Cells* **2012**, *98*, 52−56.
(24) Schumann, S.; Campo, R.; Da; Illy, B.; Cruickshank, A. C.; McLachlan, M. A.; Ryan, M. P.; Riley, D. J.; McComb, D. W.; Jones, T. S. *J. Mater. Chem.* **2011**, *21*, 2381−2386.
(25) Huang, J.; Yin, Z.; Zheng, Q. *Energy Environ. Sci.* **2011**, *4*, 3861−3877.
(26) Ameri, T.; Dennler, G.; Waldauf, C.; Denk, P.; Forberich, K.; Scharber, M. C.; Brabec, C. J.; Hinger, K. *J. Appl. Phys.* **2008**, *103*, 084506 (1)−084506(6).
(27) Abdou, M. S. A.; Orfino, F. P.; Son, Y.; Holdcroft, S. *J. Am. Chem. Soc.* **1997**, *119*, 4518−4524.
(28) Moulé, A. J.; Meerholz, K. *Appl. Phys. B: Laser Opt.* **2007**, *86*, 721−727.
(29) Tumbleston, J. R.; Ko, D.-H.; Samulski, E. T.; Lopez, R. *Phys. Rev. B* **2010**, *82*, 205325(1)−205325(8).
(30) Vandewal, K.; Tvingstedt, K.; Gadisa, A.; Inganäs, O.; Manca, J. V. *Nat. Mater.* **2009**, *8*, 904−909.
(31) Gadisa, A.; Svensson, M.; Andersson, M. R.; Inganäs, O. *Appl. Phys. Lett.* **2004**, *84*, 1609−1611.
(32) Scharber, M. C.; Mühlbacher, D.; Koppe, M.; Denk, P.; Waldauf, C.; Heeger, A. J.; Brabec, C. J. *Adv. Mater.* **2006**, *18*, 789−794.
(33) Olson, D. C.; Shaheen, S. E.; White, M. S.; Mitchell, W. J.; Hest, M. F. A. M.; van; Collins, R. T.; Ginley, D. S. *Adv. Funct. Mater.* **2007**, *17*, 264−269.
(34) Burkhard, G. F.; Hoke, E. T.; Scully, S. R.; McGehee, M. D. *Nano Lett.* **2009**, *9*, 4037−4041.
(35) (a) Quiles, M. C.-; Ferenczi, T.; Agostinelli, T.; Etchegoin, P. G.; Kim, Y.; Anthopoulos, T. D.; Stavrinou, P. N.; Bradley, D. D. C.; Nelson, J. *Nat. Mater.* **2008**, *7*, 158−164. (b) Björström, C. M.; Nilsson, S.; Bernasik, A.; Budkowski, A.; Andersson, M.; Magnusson, K. O.; Moons, E. *App. Surf. Science* **2007**, *253*, 3906−3912. (c) Song, T.; Wu, Z.; Tu, Y.; Jin, Y.; Sun, B. *Semicond. Sci. Technol.* **2011**, *26*, 034009(1)−034009(7). (d) Xue, B.; Vaughan, B.; Poh, C. H.; Burke, K. B.; Thomsen, L.; Stapleton, A.; Zhou, X.; Bryant, G. W.; Belcher, W.; Dastoor, P. C. *J. Phys. Chem. C* **2010**, *114*, 15797−15805. (e) Germack, D. S.; Chan, C. K.; Kline, R. J.; Fischer, D. A.; Gundlach, D. J.; Toney, M. F.; Richter, L. J.; DeLongchamp, D. M. *Macromoleculs* **2010**, *43*, 3828−3836.
(36) Vaynzof, Y.; Kabra, D.; Zhao, L.; Chua, L. L.; Steiner, U.; Friend, R. H. *ACS Nano* **2011**, *5*, 329−336.
(37) Cheun, H.; Berrigan, J. D.; Zhou, Y.; Fenoll, M.; Shim, J.; Hernandez, C. F.-; Sandhage, K. H.; Kippelen, B. *Energy Environ. Sci.* **2011**, *4*, 3456−3460.
(38) Lin, Y.-Y.; Lee, Y.-Y.; Chang, L.; Wu, J.-J.; Chen, C.-W. *Appl. Phys. Lett.* **2009**, *94*, 063308(1)−063308(3).
(39) Vaynzof, Y.; Kabra, D.; Zhao, L.; Ho, P. K. H.; Wee, A. T.-S.; Friend, R. H. *Appl. Phys. Lett.* **2010**, *97*, 033309(1)−033309(3).
(40) Goh, C.; Scully, S. R.; McGehee, M. D. *J. Appl. Phys.* **2007**, *101*, 114503(1)−114503(12).
(41) Gadisa, A.; Liu, Y.; Samulski, E. T.; Lopez, R. *Appl. Phys. Lett.* **2012**, *100*, 253903(1)−253903(4).
(42) Yang, T.; Wang, M.; Duan, C.; Hu, X.; Huang, L.; Peng, J.; Huang, F.; Gong, X. *Energy Environ. Sci.* **2012**, *5*, 8208−8214.